Assessment of Band Ratios and Feature-oriented principal component selection (FPCS) Techniques for Iron Oxides Mapping with relation to radioactivity using Landsat 8 at Bahariya Oasis, Egypt

El Zalaky M.A, Essam M. Esmail and El Arefy R.A

Nuclear Materials Authority, Cairo, Egypt
essam_12mem@yahoo.com

Abstract: Iron is an important element in mineral exploration using remote sensing techniques in part because of its overall abundance in the crust, about 8%, and its abundance and occurrence in rock and minerals of economic importance. The Bahariya Oasis area of the western desert of Egypt is well known by iron mining activity from long time in certain locations. Number of remote sensing techniques have been accomplished and tested using Landsat 8 Operational Land Imager (OLI) imagery data covering the Bahariya Oasis for elucidating iron oxides exposures, such as image composite, band ratios, principal component analysis (PCA) methods. Principal component analysis techniques; known as Feature-oriented Principal Component Selection (FPCS), used for discriminations of iron oxides, including selective and developed selective principal component methods respectively. The assessment of iron oxides new proposed band ratios (7/5+3/4) and (b4/ (b1+b2)), and the separability of the PCA techniques, support the findings and proposed some new exposed localities. The results showed that Landsat 8 OLI can effectively discriminate iron oxides groups due to the presence of five bands in VNIR and two SWIR bands with a high radiometrically resolution, in addition to its better availability and spatial coverage makes Landsat 8 sensor more suitable for large area lithologic mapping.

[El Zalaky M.A, Essam M. Esmail and El Arefy R.A**. Assessment of Band Ratios and Feature-oriented principal component selection (FPCS) Techniques for Iron Oxides Mapping with relation to radioactivity using Landsat 8 at Bahariya Oasis, Egypt.** *Researcher* 2018;10(4):1-10]. ISSN 1553-9865 (print); ISSN 2163-8950 (online). http://www.sciencepub.net/researcher. 1. doi:10.7537/marsrsj100418.01.

Keywords: Bahariya Oasis; Iron oxides; Landsat 8 OLI; PCA; Feature Oriented Principal Component Selection; Band ratios.

Introduction

Bahariya Oasis area attracted attention since the discovery of some radioactive anomalies in its northern part, especially at the base of El Gidida iron ore deposit in 1978. In the same year, a field party from the Egyptian Nuclear Materials Authority (NMA) discovered uranium-mineralization at G. El Hufhuf (Hussein et al., 1979). Since then, extensive exploration of the Bahariya Oasis for radioactive mineralization resulted in the discovery of large number of radioactive anomalies (Morsy, 1987). El-Akkad and Issawi (1963) suggested that the iron ore at El Gedida, Nasser, Ghorabi, and El-Harra areas were formed partially as a result of shallow marine deposition and partially with surface replacement of the carbonate after their deposition in the shallow depression. The economic iron deposits of El Bahariya Oasis are confined to Karst features, and it is suggested that they were formed through lateritization processes during the senile stage of a post- Eocene Karst event. El Aref (1999) recognized successive types of iron ore formed under sub-aerial and shallow marine conditions at Bahariya Oasis; these are: Cenomanian strata including iron stone in strata-bound iron-rich laterite, Lutetian strata including pisolitic-oolitic ironstone, Lutetian stratiform mudstone, and stratabound karst ore from paleo-karstification processes. Salama et al. (2013) mentioned that preitidal ferruginous microbialites form the main bulk of the middle Eocene ironstone of the Bahariya area.

Space-borne multispectral systems such as Landsat MSS, TM, and the recent launched Landsat 8 have four to eleven spectral bands (channels) that can be utilized for structural and geomorphic features at the regional map scale, and also used to identify alteration associated mineral deposits (Abrams et al., 1983; Goetz et al., 1983; Perry, 2004). Landsat Thematic Mapper TM imagery has been used for mineral exploration because the two-shortwave infrared (SWIR) bands that may be useful for identifying alteration mineral assemblages (Abdelsalam et al., 2000; Sabins, 1999). Iron's abundance and chemical reactivity under oxidizing conditions of the Earth's oxygen-rich atmosphere makes it an important contributor to minerals formed by chemical weathering at or near the earth's surface on rock and mineral surfaces, and in aqueous solution from which minerals precipitate (Kesler and Laznicka, 1994).

The most common absorption bands in the 0.4-2.5µm wavelength region are caused by ferric (Fe^{3+}) and ferrous (Fe^{2+}) iron ions in iron oxides and mafic silicates, the hydroxyl (OH-1) ion in hydroxides and

clays, H_2O in hydrated minerals, the carbonate CO_{3-2} ion in carbonate minerals, and the sulfate SO_{4-2} ion in sulfate minerals (Vincent, 1997). Ferrous iron (Fe^{2+}) produces electronic absorptions centered at about 0.45 µm, 1.0–1.1 µm, 1.8–1.9 µm, and 2.2–2.3 µm, depending on its lattice environment. Ferric iron (Fe^{3+}) produces absorptions at wavelength number between of 0.65 µm and 0.87 µm. Visible and short-wavelength real infrared absorptions cause vibrational bending and stretching of bonds within radicals or molecules (Abrams et al., 1988; Rajendran et al., 2011).

The Crosta technique is also known as Feature Oriented Principal Component Selection (FOPCS) or developed selective PCA method. Through the analysis of the eigenvector values it allows identification of the principal components that contain spectral information about specific minerals, as well as the contribution of each of the original bands to the components in relation to the spectral response of the materials of interest. This technique indicates whether the materials are represented as bright or dark pixels in the principal components according to the magnitude and sign of the eigenvector loadings. This technique can be applied on four and six selected bands of Thematic Mapper (TM) data (Crosta and Moore, 1989; Loughlin, 1991; Ruiz-Armenta and Prol-Ledesma, 1998). The present study tends to apply remote sensing techniques such as band ratios and FOPCS for mapping the spatial distributions of iron oxides in relation to radioactivity at Bahariya Oasis area where the hematite was deposited as iron ore from the ferric oxides which altered in parts to goethite and hydrated to hydro-goethite valuable iron ore.

Study Area and Geologic Background

The Bahariya Oasis is a large depression in the Western Desert at a distance of about 270 Km SW of Cairo and 180 Km west of the Nile Valley. The geology of the area is relatively well known and has been studied by several investigators since 1903. The surface and subsurface successions of Bahariya Oasis have been investigated by several authors (El-Akkad and Issawi, 1963; El Arafy, 2010; El Mansy et al., 1989; Khalifa et al., 2002; Morsy, 1987; Moustafa et al., 2003; Said, 1962; Salem, 1995; Soliman and El Badry, 1980; Soliman and El Badry, 1970). The idealized sedimentary columnar section in Bahariya Oasis has a thickness nearly about 2000 m and ranges from Cambrian to Oligocene and covered by some Quaternary deposits (Salem, 1995). From this sedimentary section, about 200 to 300 m are outcropping on the surface especially in the northern part of the oasis.

The exposed rocks of the Bahariya Oasis and its surrounding plateau range in age from Cenomanian to Middle Miocene. They are of sedimentary origin except for basalt flows and dolerite sills and dykes (Fig. 1).

The assigned age of the Bahariya Formation which covers the floor of the depression is Early to Late Cenomanian (El bassyony, 2004; Said, 1962). The formation is exposed on the surface and forms the floor and part of scarps and hills with a cumulative thickness 209 m in the Bahariya Oasis (Soliman and El Badry, 1970). The iron ore of El Harra belongs to El Harra member of El Haffuf Formation; whereas El Gedida iron ore belongs to Naqb Formation as shown in Figure 1.

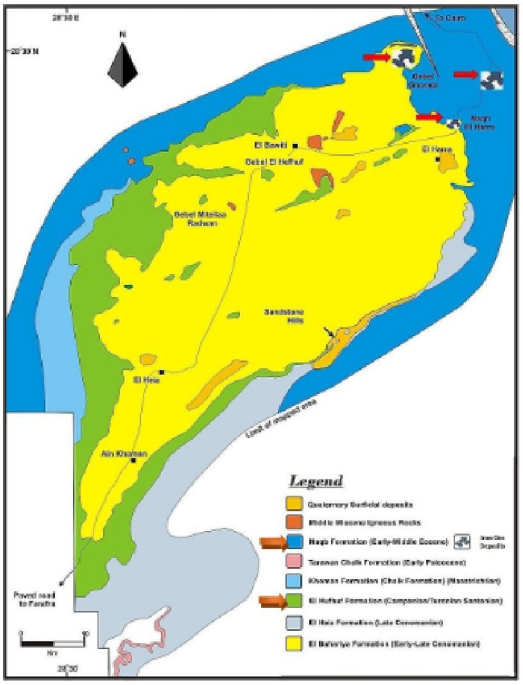

Fig. 1. Simplified geological map of the Bahariya Oasis modified from (El Arafy, 2010; Moustafa et al., 2003)

Regarding to the main structural features; the depression of Bahariya Oasis is an anticline of considerable extent oriented NE/SW, a typical structure of the Syrian Arc belt. The axis of this great anticline runs in a southwest trend from Gebel Ghorabi in the north, past the central hills of the depression to the southern part of the oasis, and seems to continue south to include the Farafra structure. Many authors studied the surface structures of Bahariya Oasis (El-Akkad and Issawi, 1963; El-Bassyouny, 1978; El-Etr and Moustafa, 1976; Morsy, 1987; Moustafa et al., 2003; Said, 1962; Salem, 1995). The iron ore is thought to be localized in the crests of two major anticlines trending in a NE direction. El Gedida and El Harra iron ore deposits

are localized on the eastern anticline, on the other hand Ghorabi and Nasser iron ore deposits are on the western anticline. The high grad ores exist in the crests while the low-grade ores are founded in the limbs of the anticlinal structures.

2. Data and Methodology

One of the latest successful remote sensing platforms is Landsat 8, an American Earth Observation satellite launched on February 11, 2013. The Landsat 8 satellite carries a two-sensor payload, the Operational Land Imager (OLI) and the Thermal Infrared Sensor (TIRS), described in detail in Irons et al. (2012) and summarized in Table 1 for OLI sensor. The absorption and reflectance spectra of altered rocks and ferrous minerals can be resolved in Landsat 8 OLI data and processed to detect and display these rocks and minerals within a scene. Some silicate minerals may be detected through two additional thermal bands (Dehnavi et al., 2010; Pour and Hashim, 2011).

Table 1. Landsat 8 OLI Sensor (VNIR-SWIR) Parameters.

Subsystem	Spectrum	Band No	Spectral Range (μm)	Spatial Resolution (m)	Quantization levels
OLI	VNIR	1	0.435 - 0.451	30	16 bit
		2	0.452 - 0.512		
		3	0.533 - 0.590		
		4	0.636 - 0.673		
		5	0.851 - 0.879		
	SWIR	6	1.566 - 1.651		
		7	2.107 – 2.294		

In the present study, the OLI Landsat 8 cloud-free scene (Path 178 and Row 40) acquired on 12 August 2017 at 08:36 am local time covering the investigated area, have been radiometrically and geometrically corrected in UTM projection WSG84, with spatial resolutions of 30m.

Two main digital image processing techniques have been applied to the Landsat 8 OLI data covering the area in order to elucidate the spatial distribution of iron oxides at the Bahariya Oasis area. The first image processing technique applies band-ratio method by dividing the digital number (DN) values of one band by the corresponding DN values of another band and displaying the new DN values as a grayscale image (Sabins, 1999). This image processing technique emphasizes the differences between spectral features meanwhile neglects common features. In addition, it helps in removing shadows and illumination contrasts caused by feature slope (Sabins, 1999) as in the case of El Bahariya scarps. The band ratios selection for bands depends on the spectral characteristic of the exposed rock units and minerals Figure 2.

The second image processing technique is the principal components analysis (PCA). Three PCA techniques, used for The Landsat 8 OLI data, were the standard *PCA* on seven reflective bands, *selective PCA* on two bands, and *developed selective PCA (Crosta technique)* or *Feature-oriented Principal Components Selection (FPCS)* on four bands.

The Principal Components Analysis *PCA* is a common method for enhancement of the alteration haloes surrounding the porphyry intrusive bodies responsible for the mineralization of porphyry deposits where all 7 reflective Landsat 8 OLI bands are considered as input to calculate principal component analysis procedure. The first principal component image will have the information that is common to all bands used as input to PCA. Overall scene brightness, or albedo is responsible for the strong correlation between multispectral image channels. The remaining components should therefore account for decreasing variance caused by differences between spectral regions and between individual bands.

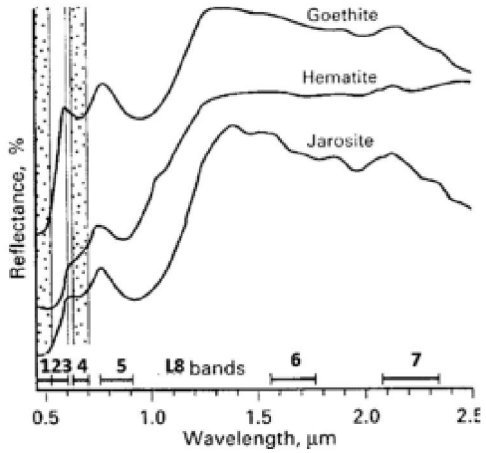

Fig. 2. Spectral reflectance curves for iron oxide minerals goethite, hematite and jarosite showing sharp fall-off in reflectance in the UV-blue region (bands 1, 2 and 4 in Landsat 8) due to the charge-transfer effect, modified from (Hunt and Ashley, 1979a; Sabins, 1999).

In case of *selective PCA*, only a subset of multispectral bands is used as input to PCA. This

method is useful for dimensionality reduction while minimizing the amount of information lost to unused components (Chavez et al., 1982; Kwarteng and Chavez, 1989). The two input bands are selected according to the spectral characteristics of hydrous minerals, and hence many hydrothermally altered rocks (Kaufman, 1988). By using only two images/bands as input, the information that is common to both will be mapped to the first component PC1 and information that is unique to either one of the two images will be mapped to the second component PC2 which makes results easier to visually interpret.

Crosta and Moore (1989) described a methodology called *Feature-oriented Principal Components Selection (FPCS)* or *developed selective* method. FPCS is based on the examination of PCA eigenvector loadings to decide which of the principal component images will concentrate information directly related to the theoretical spectral signatures of specific targets. An important aspect of this approach is that it predicts if the target surface type is highlighted by dark or bright pixels in the relevant principal component image and can be showing using different color draping such as rainbow and with stretching data or not according to the operator. A modified form of PCA, which uses sets of four selected image bands is developed for delineating hydroxyl and iron-oxide alteration zones (Loughlin, 1991).

Field investigation has been accomplished in order to investigate the findings and localities during and after the image processing techniques applied. Radioactive field measurements have been carried on the iron oxides exposures with special interest in the new localities at El Harra and South areas.

3. Results and Discussion

Landsat 8 OLI bands are too wide to allow the identification of single minerals; however, they serve to identify groups of minerals for exploration purposes in the near and middle infrared, belonging to the hydroxyl and Iron oxide. These minerals have spectral features in the visible and infrared parts (0.4 - 2.5 µm). Absorption anomalies at wavelengths less than 0.9 µm are a good indication of hematite. When the anomalies are at wavelengths above 0.9 µm, jarosite or goethite are more abundant (Hunt and Ashley, 1979b). Preprocessing of the image included radiometric correction to remove the atmospheric effects.

- Color composite image:

False color composites included the bands where the spectral response of the minerals indicates a maximum in their reflectance. This enhancement is achieved by combining bands in the visible and the infrared (Crosta and Moore, 1989). The combinations are suitable for identifying and distinguishing major geologic units and topographic features. It can be differentiated by their tones where the iron ore of El Gidida mine, Naqeb El Harra and G. Ghoraby areas appeared as dark brown color in the natural color combination 432 (Fig 3 left) and red to dark magenta in the false color combination (Fig 3 right) due to their rich in iron oxides composition. On the other hand, it is clearly that the cultivated areas displayed as a black color (Fig. 3 left) and green color (Fig. 3 right).

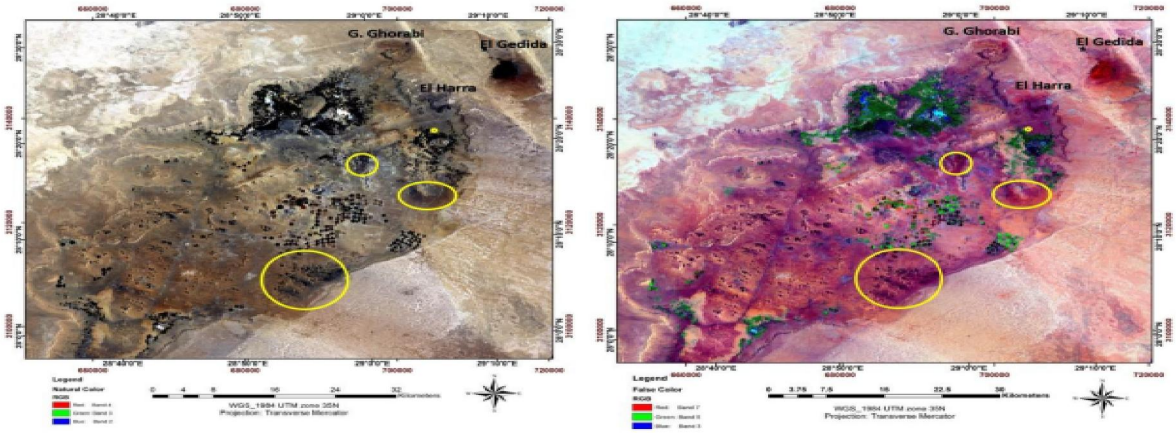

Fig. 3. Color composite image of 4, 3, 2 (left) and 7; 5; 3 (right) displayed in RGB respectively delineate the areas rich by iron oxides (yellow circles).

- Band ratios:

Two new proposed band ratios were used to discriminate the distribution of iron oxides all over the studied area. The first one band 4 / (band 1+ band 2) of Landsat 8 OLI displayed as color image using color table (Fig. 4). The ratio applied successfully for

mapping and discriminating the three iron mine areas (El Gidida, Naqeb El Harra and G. Ghoraby) as red color. The distinguishing was due to its sensitivity to specific chemical and mineralogical composition of the rock carrying the iron. It is also emphasizing and discriminate three more localities that most probably have the same composition of the previously discovered iron ore areas. These areas are appeared by red color and delineated by back circles in Figure 4.

The ratio remarkably showed the cultivated lands and vegetated areas inside the depression as a red color and it may be as a result of the enrichment of the soil and irrigated underground water with high iron and manganese concentrations (El Arafy, 2010).

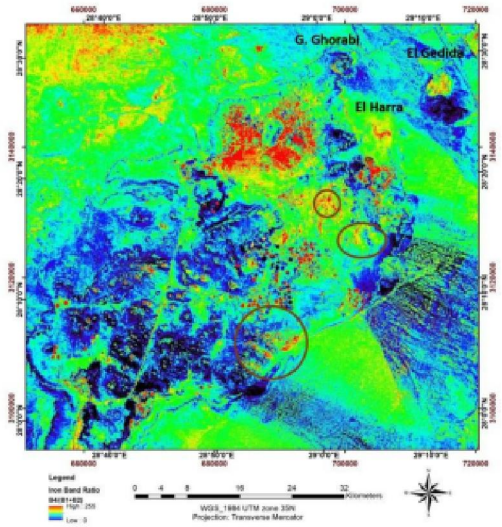

Fig. 4. A new proposed band ratio b4/(b1+b2) delineate the areas rich by iron oxides (black circles).

The second new proposed band ratio is (band 7 / band 5) + (band 3 / band 4) of Landsat 8 OLI that depend mainly on band 4 and band 5 to differentiate areas of iron oxides from areas of vegetation (Ducart et al., 2016). This band ratio helped in recognizing the distribution and concentrations of the iron ore in the study area. This band ratio displayed as color image whereas the iron provided as dark red, red and yellow colors depending on iron concentration, where the maximum concentration of iron appears as dark red color and the minimum as yellow color (Fig. 5). The advantage of this ratio is to suppress the cultivated area which appeared by dark gray color.

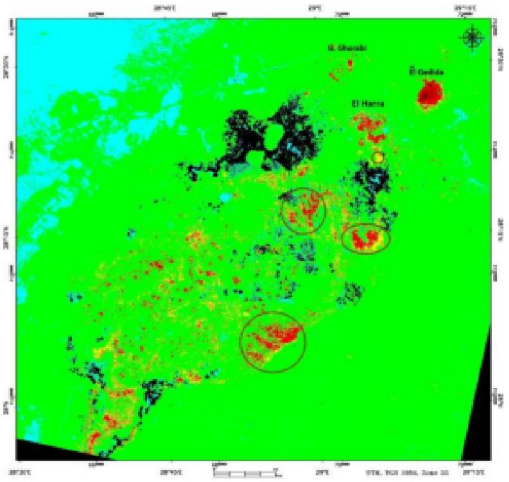

Fig. 5. Band ratio (b7/b5)+(b3/b4) displayed as color image delineate the areas rich by iron oxides (dark red, red and yellow color).

- Principal component analysis (PCA):

The application of PC transformation for mapping iron oxides zones applied through three techniques named: Standard, Selective and Feature Oriented (Developed selective) PCA.

Standard PC transformation was conducted for the study area using correlation coefficient of the same input 7 bands covering Bahariya Oasis (Table 2). The first PC mapped albedo and topographic information. Study of the individual PC images revealed that eigenvectors of PCs 1, 2, 4 and 6 display contrasting response for iron oxides better. This gave PC 6, 4, 1 in RGB respectively (Fig. 6), as the composite with maximum spectral contrast shown the distribution of iron oxides in the depression as reddish color.

Table 2. Correlation coefficient used for standardized PC transformation.

Eigenvectors	*PC 1*	*PC 2*	PC 3	*PC 4*	PC 5	*PC 6*	PC 7
Band 1	0.16	0.19	0.30	0.40	0.43	0.54	0.46
Band 2	0.32	0.34	0.36	0.24	0.34	-0.38	-0.58
Band 3	-0.27	-0.28	-0.29	-0.30	0.81	0.05	-0.16
Band 4	-0.40	-0.28	0.15	0.47	0.11	-0.61	0.36
Band 5	-0.39	-0.32	0.05	0.49	-0.17	0.43	-0.54
Band 6	-0.27	-0.16	0.81	-0.49	-0.04	0.07	0.00
Band 7	0.65	-0.75	0.09	0.04	0.01	-0.02	0.01

In selective methods, the first and second PC of the following pairs of Landsat 8 OLI bands were generated (Fig. 7):

1- band 2 and band 4
2- band 2 and band 6
3- band 2 and band 7

These pairs were selected based on the spectral signatures of iron oxides minerals and mapping the spectral contrast that shows surface iron distributions. The first two pairs were chosen because the third pairs with input bands 2 and 7 gave almost the same result of the second pairs with input bands 2 and 6. By using selective PC with only two bands as input, the second component has information that is unique either one of the bands, while first component shows information that is common to both bands (Kwarteng and Chavez, 1989). In case of first pairs (bands 2 and 4) the iron is distinctively appeared in the first component (Fig. 7A), while in the second pairs (bands 2 and 6) both PC 1 and 2 distinguished the iron distribution (Fig. 7 B & C).

The Crósta technique/Feature-oriented (FPCS) or developed selective PC has been applied to Landsat 8 OLI processed image by selecting certain spectral bands (b2, b4, b5, & b6), that equivalent to Landsat TM bands (b1, b3, b4 & b5) used by Loughlin (1991), to detect the spectral information of iron oxide minerals. By analyzing FPCS statistics (Table 3), PC1 shows a high positive loading from band 6 (0.75) and high negative loading from band 4 (-0.39), this indicates that iron oxides will appear as bright pixels in the grayscale image. Whereas, PC4 has a strong positive loading with band 4 (0.73) and strong negative loading with band 1 (-0.65); this indicates that iron oxides will appear as dark pixels in PC4 image. The gray scale interpretation shows PC1 and PC4 are remarkable to iron oxide concentration as bright pixels (Fig. 8).

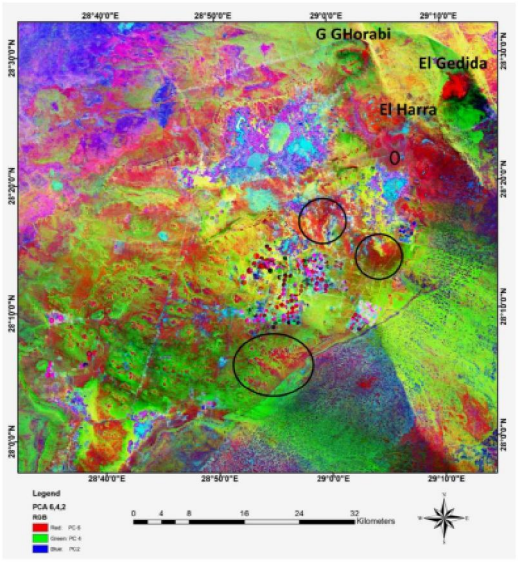

Fig. 6. Composite image of PC 6,4,1 as RGB.

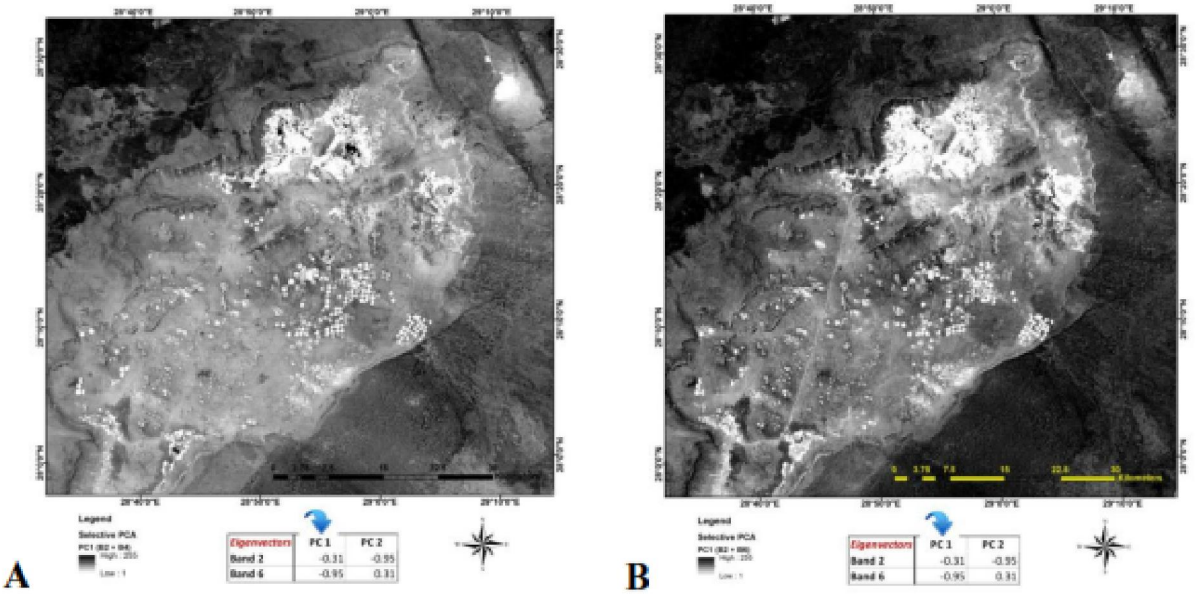

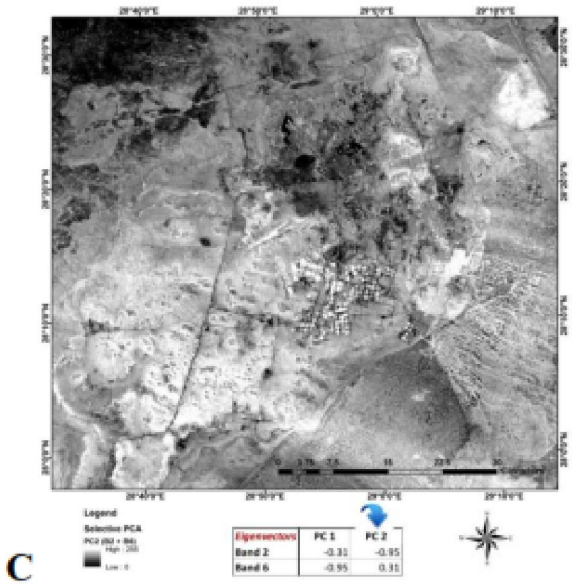

Fig. 7. Principal component: A) number one spectral contrast image of input bands 2 and 4. B) number one spectral contrast image of input bands 2 and 6 of Landsat 8 OLI. This image isolates/maps the areas containing iron oxides in brightness.

Table 3. Eigenvector loadings of Bahariya Oasis scene for iron-oxides mapping using Landsat 8 OLI bands 2, 4, 5 and 6.

Eigenvectors	***PC 1***	**PC 2**	**PC 3**	***PC 4***
Band 2 ↓	-0.23	-0.49	-0.53	-0.65
Band 4 ↑	-0.39	-0.21	-0.53	0.73
Band 5 ↓	0.48	0.57	-0.66	-0.06
Band 6 ↑	0.75	-0.63	-0.01	0.21

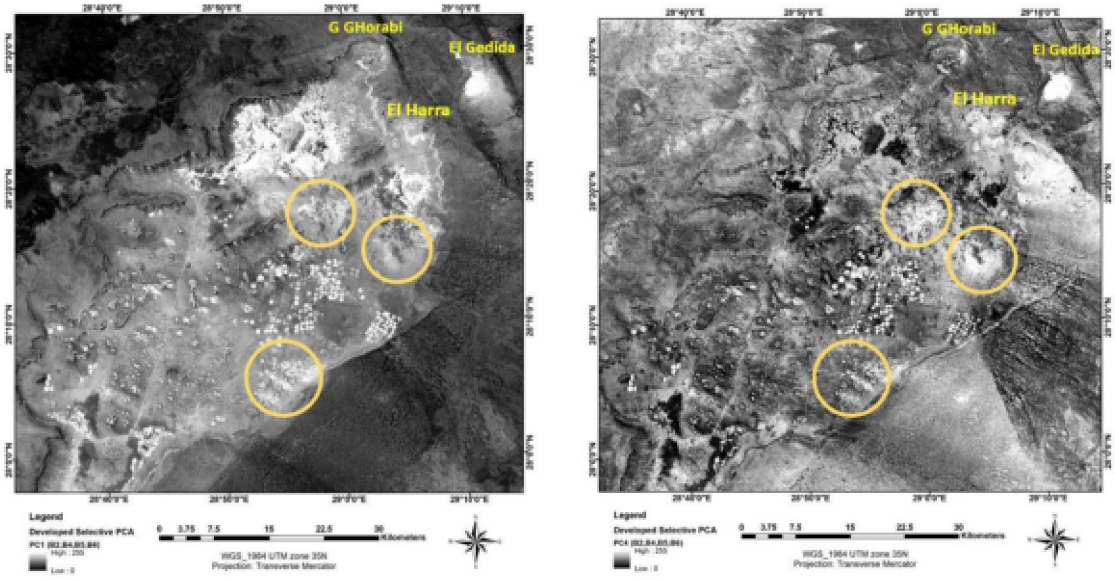

Fig. 8. Grayscale image of PC1 and PC4 for selected Landsat-8 bands showing and discriminate the iron oxides in three areas (yellow circles)

Based on remotely-sensed results and their interpretation, an intensive geological field work to validate results given by remote sensing was performed during the current study. Samples from rock varieties in the study areas were collected for analytical techniques. This field study identified four areas with different concentration of iron-oxides located at different localities all over the study area. One of these localities is located north El Harra village and its extension is very small and less concentrated in iron oxide (Fig. 9A). These rocks are present mainly in the form of small layer of ferruginated marly limestone.

The second and third areas are located south and west of El Harra village. The ferruginous units represented by hard and massive ferruginous quartzitic sandstone intercalated with highly altered hematinic layers of mud and clay (Fig. 9 B, C and D) respectively.

The siliciclastic beds of the Bahariya Formation are weathered into black conical-like hills, mesas, and buttes. The black conical hills, which are distributed on the southern part of the Bahariya Depression (southern yellow circle), are known as “Black sandstone hills”. Most of these hills are capped by ferruginous sandstone, giving them a characteristic black color (Fig. 9 (E).

All the detected ferruginous rock units were subjected to field radioactive measurements. After calibration processes of the portable gamma-ray spectrometer (Gamma Gun FD-3013) (Fig. 9 D) at NMA laboratory eU Calibration Pad. During this survey, almost all lithological units exposed within and around these localities were more or less covered and radiometrically surveyed. Particular attention was paid to all the zones that contain highly concentration of the iron oxides. Table (4) summarize the measured radioactivity expressed in eU ppm. These field background radioactivity levels for ferrugenated localites show very low range and this may be due to that these areas are exposed to meteoric water that leached the surfacial uranium

Concluding Remarks

The interpretations of different kind of remote sensing techniques of Landsat 8 data partially succeeded in identifying the ferruginous units as ironstone, ferruginous quartzitic sandstone, ferruginous marly limestone as well as ferruginous clay at different localities at Bahriya Oasis. These iron oxide localities were also measured radioactivity and reviled that the concentration of eU all over the studied localities are within the low grade concentration.

Further detailed geological field work on the basis and contribution and geochemical and geophysical analyses are recommended. Finally, the area has significant potential for surface and subsurface iron oxides.

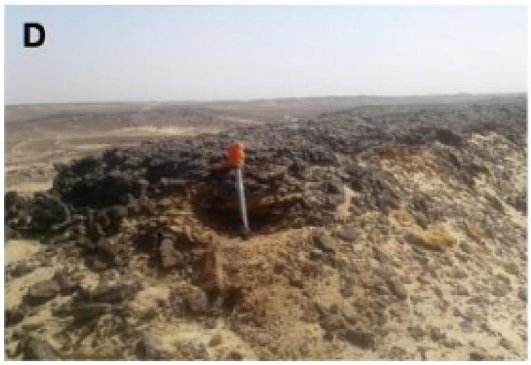

Fig. 9: (A) lens of ferruginated marly limestone North El Harra village, (B) ferrugenated sand and clay West El Harra village (C and D) ferrugenated and massive quartzitic sandstone measured by Gamma Gun Radiometric Tool (E) black conical-like hills of ferruginous sandstone at southern parts of El Bahariya Oasis.

Table 4: Field gamma-ray radioactivity eU (ppm) for all the detected ferruginated units exposed in the study area using a portable Gamma-Gun spectrometer (model FD-3013).

LOCALITIES	eU (ppm)	
	Range	**Average**
NORTH EL HARRA VILLAGE	20 - 60	32
WEST EL HARRA VILLAGE	18 - 35	26
SOUTH EL HARRA VILLAGE	10 - 25	17.5
SOUTHERN PART OF BAHARIYA OASIS	35 - 55	43.5

References

1. Abdelsalam, M. G., Stern, R. J., and Berhane, W. G., 2000, Mapping gossans in arid regions with Landsat TM and SIR-C images: the Beddaho Alteration Zone in northern Eritrea: Journal of African Earth Sciences, v. 30, no. 4, p. 903-916.
2. Abrams, M., Rothery, D., and Pontual, A., 1988, Mapping in the Oman ophiolite using enhanced Landsat Thematic Mapper images: Tectonophysics, v. 151, no. 1- 4, p. 387-401.
3. Abrams, M. J., Brown, D., Lepley, L., and Sadowski, R., 1983, Remote sensing for porphyry copper deposits in southern Arizona: Economic Geology, v. 78, no. 4, p. 591-604.
4. Chavez, P., Berlin, G. L., and Sowers, L. B., 1982, Statistical method for selecting landsat MSS: J. Appl. Photogr. Eng., v. 8, no. 1, p. 23-30.
5. Crosta, A., and Moore, J., 1989, Enhancement of Landsat thematic mapper imagery for residual soil mapping in SW Minais Gerais atate, Brazil: a prospecting case history in Greenstone belt terrain, in: proceedings of the Seventh ERIM Thematic Conference: Remote sensing for Exploration Geology, p. 1173-1187.
6. Dehnavi, A. G., Sarikhani, R., and Nagaraju, D., 2010, Image processing and analysis of mapping alteration zones in environmental research, East of Kurdistan, Iran: World Applied Sciences Journal, v. 11, no. 3, p. 278-283.
7. Ducart, D. F., Silva, A. M., Toledo, C. L. B., and Assis, L. M. d., 2016, Mapping iron oxides with Landsat-8/OLI and EO-1/Hyperion imagery from the Serra Norte iron deposits in the Carajás Mineral Province, Brazil: Brazilian Journal of Geology, v. 46, no. 3, p. 331-349.
8. El-Akkad, S., and Issawi, B., 1963, Geology and iron ore deposits of the Bahariya Oases: Geol. Surv. and Min. Res. Dept, Cairo, Egypt, Paper, no. 18.
9. El-Bassyouny, A., 1978, Structure of the northeastern plateau of the Bahariya Oasis, Western Desert, Egypt: Geol Mijnb, v. 57, p. 77-86.
10. El-Etr, H. A., and Moustafa, A. R., 1976, Utilization of orbital imagery and conventional aerial photography in the delineation of the regional lineation pattern of the cetnral western desert of Egypt with a particular emphasis on the Bahariya region, Ain Shams University.
11. El Arafy, R. A., 2010, Composition and radioactivity of groundwater and some quaternary sabkha sediments in Bahariya Oasis, Egypt [M.Sc.: Mansoura University, 192 p.
12. El Aref, M., GAW4, Int. Conf. on Geol. of the Arab World, Cairo Univ., Egypt, 1999, 10-22, *in* Proceedings Geology of the Arab World, 1999: Proceedings of the Fourth International Conference on Geology of the Arab World, Cairo University, Egypt, 19981999, Volume 1, Geology Department, Faculty of Science, Cairo University.
13. El bassyony, A., 2004, Stratigraphy of El Harra Area, Bahariya Oases, Western Desert, Egypt:

Journal of the Sedimentological Society of Egypt, v. 12, p. 207-232.
14. El Mansy, I. M., Ragab, M. A., and EI Gendy, N. H., 1989, Studies on petrologic and petrophyscal properties of some Cambrian and lower Cretaceous core samples from Bahariya Oasis Western Desert Egypt: Science Journal Faculty of Science Menoufia University, v. 3, p. 285-304.
15. Goetz, A. F., Rock, B. N., and Rowan, L. C., 1983, Remote sensing for exploration; an overview: Economic Geology, v. 78, no. 4, p. 573-590.
16. Hunt, G. R., and Ashley, P., 1979a, Spectra of altered rocks in the visible and near infrared: Ecol. Geol., v. 74, p. 1613-1629.
17. Hunt, G. R., and Ashley, R. P., 1979b, Spectra of altered rocks in the visible and near infrared: Economic Geology, v. 74, no. 7, p. 1613-1629.
18. Hussein, H. A., Hassan, M. A., Meshref, W. M. A., and El Hazek, N. T., 1979, Verification of radiometric anomalies in Bahariya Oasis locality, Western Desert, Egypt: NMC.
19. Irons, J. R., Dwyer, J. L., and Barsi, J. A., 2012, The next Landsat satellite: The Landsat Data Continuity Mission: Remote Sensing of Environment, v. 122, p. 11-21.
20. Kaufman, H., 1988, Mineral exploration along the Agaba-Levant structure by use of TM-data concepts, processing and results: International Journal of Remote Sensing, v. 9, p. 1630–1658.
21. Kesler, S., and Laznicka, P., 1994, Mineral Resources, Economics, and the Environment: Ore Geology Reviews, v. 9, no. 6, p. 511-512.
22. Khalifa, M., Soliman, H., and Abu El Hassan, M., Lithostratigraphy and sequence stratigraphy of the Turonian–Santonian rocks, Bahariya Oasis, Western Desert, Egypt, *in* Proceedings The 6th conference of the Geological Arab World, Cairo University 2002, p. 483-500.
23. Kwarteng, A., and Chavez, P. S. J., 1989, Extracting spectral contrast in Landsat Thematic Mapper image data using selective principal component analysis: Photogramm. Eng. Remote Sens, v. 55, p. 339-348.
24. Loughlin, W. P., 1991, Principal Component Analysis for alteration mapping: Photogrammetric Engineering and Remote Sensing, v. 57, p. 1163-1169.
25. Morsy, M., 1987, Geology and radioactivity of Late Cretaceous-Tertiary sediments in the Northern Western Desert, Egypt: Ph. D. Thesis, Fac. Sci, Mansoura Uni., Egypt.
26. Moustafa, A. R., Saoudi, A., Moubasher, A., Ibrahim, I., Molokhia, H., and Schwartz, B., 2003, Structural setting and tectonic evolution of the Bahariya Depression, Western Desert, Egypt: GEOARABIA-MANAMA-, v. 8, p. 91-124.
27. Perry, S. L., 2004, Spaceborne and airborne remote sensing systems for mineral exploration-case histories using infrared spectroscopy: Infrared spectroscopy in geochemistry, exploration geochemistry, and remote sensing, p. 227-240.
28. Pour, A. B., and Hashim, M., 2011, Identification of hydrothermal alteration minerals for exploring of porphyry copper deposit using ASTER data, SE Iran: Journal of Asian Earth Sciences, v. 42, no. 6, p. 1309-1323.
29. Rajendran, S., Thirunavukkarasu, A., Balamurugan, G., and Shankar, K., 2011, Discrimination of iron ore deposits of granulite terrain of Southern Peninsular India using ASTER data: Journal of Asian Earth Sciences, v. 41, no. 1, p. 99-106.
30. Ruiz-Armenta, J. R., and Prol-Ledesma, R. M., 1998, Techniques for enhancing the spectral response of hydrothermal alteration minerals in Thematic Mapper images of Central Mexico: International Journal of Remote Sensing, v. 19, p. 1981-2000.
31. Sabins, F. F., 1999, Remote sensing for mineral exploration: Ore Geology Reviews, v. 14, no. 3–4, p. 157-183.
32. Said, R., 1962, The geology of Egypt, pp. 377: Eisvier, Amsterdam-New York.
33. Salama, W., El Aref, M., and Gaupp, R., 2013, Mineral evolution and processes of ferruginous microbialite accretion–an example from the Middle Eocene stromatolitic and ooidal ironstones of the Bahariya Depression, Western Desert, Egypt: Geobiology, v. 11, no. 1, p. 15-28.
34. Salem, A. A., 1995, Groundwater conditions in the Bahariya oasis and its future development [M.Sc.: Cairo University, p.132.
35. Soliman, S., and El Badry, O., 1980, Petrology and tectonic framework of the Cretaceous, Bahariya Oasis, Egypt: Journal of Geology, v. 24, p. 11-51.
36. Soliman, S. M., and El Badry, O., 1970, Nature of Cretaceous sedimentation in western desert, Egypt: AAPG Bulletin, v. 54, no. 12, p. 2349-2370.
37. Vincent, R. K., 1997, Fundamentals of Geological and Environmental Remote Sensing: Upper Saddle River, NJ: Prentice-Hall, Inc.

4/16/2018